THE JOURNAL OF PHYSICAL CHEMISTRY LETTERS
A JOURNAL OF THE AMERICAN CHEMICAL SOCIETY

pubs.acs.org/JPCL

Letter

Orbital Dependence in Single-Atom Electrocatalytic Reactions

Yanan Wang, Yingzong Liang, Tao Bo, Sheng Meng,* and Miao Liu*

Cite This: *J. Phys. Chem. Lett.* 2022, 13, 5969−5976

Read Online

ACCESS | Metrics & More | Article Recommendations | Supporting Information

ABSTRACT: Transition metal single-atom catalysts supported on N-doped graphene (TM−N−C) could serve as an ideal model for studying orbital dependence in electrocatalytic reactions because the atom on the catalytic active site has discrete single-atom-like orbitals. In this work, the catalytic efficiency of Fe−N−C for the oxygen evolution reaction (OER) under a small structural perturbation has been comprehensively investigated with density functional theory calculations. The results suggest that the subtle local environment of a single atom can significantly modulate the catalytic reactivity. Further analysis demonstrates that the energy level of the TM d_{z^2} orbital center, rather than the d-band center, is responsible for the OER catalytic efficiency as the d_{z^2} orbital participates mainly in the reactions. Essentially, the d-band theory can be extended to the sub-d orbital level, and a small perturbation of the crystal field, induced by lattice strain or *z*-direction displacement of the TM atom, can prominently change the sub-d orbital associated with the reaction and in turn affect the catalytic activity.

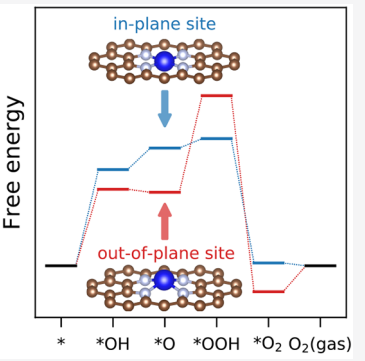

In chemical catalysis, the d-band model proposed by Hammer and Nørskov has been proven to be extremely successful in understanding bond formation and predicting the reactivity trends on transition metal surfaces (TMS).[1−6] On the basis of the Newns−Anderson model and effective medium theory, the d-band model proves that the d-band center is a fairly effective descriptor for the activity of different ligands and/or molecules on a variety of TMS.[7−11] When atoms or simple molecules are adsorbed onto TMS, bonding and antibonding states are formed below the adsorbate valence states and above the TMS d states. The strength of the interaction between the adsorbate and TMS depends on the filling of the antibonding states, and the filling in turn is given by the energy of the antibonding state relative to the Fermi level. Because the d-band center correlates well with the position of the upper d-band edge, the d-band center rules the energy position and filling of the adsorbate−metal antibonding states. Hence, the variation in the adsorption energy of the adsorbate on different TMS is correlated with their d-band center with respect to the Fermi energy. The shallow d-band center in energy relative to the Fermi level suggests the increased bond energy, vice versa. In addition to pure TMS, the d-band model has also been extended to many other transition metal (TM) systems, such as uniform coatings and heterogeneous surface layers of TM alloys, TMS with steps and strains, and TMS with toxic substances and accelerators.[12,13] In recent years, improved descriptors other than the d-band model have been sought. Vojvodic et al. found that the upper-edge position of the d states[14] can serve as a good descriptor of the absorption energy as an extended version of the d-band model. Bhattacharjee et al. proposed the spin-polarized d-band center model for TMS with a large spin polarization by considering two d-band centers.[15]

According to the molecular orbital bonding framework, the interaction between the adsorbed molecular orbitals and the surface orbitals needs to meet the symmetric matching and maximum overlap principles; hence, the adsorbate−surface interaction is dependent on the orbital. Suntivich et al. report that the e_g orbital occupancy of surface TM ions is an excellent descriptor for the oxygen evolution reaction (OER) activity of the perovskite oxides, as the σ-bonding e_g orbital, other than the π-bonding t_{2g} orbital, of surface TM ions overlaps more with the oxygen-related adsorbate.[16] In fact, the early version of d-band theory hints at the existence of orbital dependence, which is inexplicitly contained in the coupling matrix.[3] Previously, the catalysis community mainly studied the metals and ionic compounds,[17−23] in which the d orbitals form broadened bands. It is difficult to distinguish the contribution of each sub-d orbital in catalytic reactions. In single-atom catalysts (SACs), the orbitals split into discrete single-atom-like energy levels, so that it becomes easier to capture the orbital dependence in the catalytic reaction.[24−28] Clearly analyzing the orbital dependence requires a simple and highly symmetric atomistic configuration in real space to decouple each orbital; e.g., if orbitals are aligned with the direction of the adsorbate−catalyst bond, they are likely to make contributions to this very bond. Moreover, the regulatory mechanism should be simple. Fortunately, TM single-atom catalysts supported on N-doped graphene (TM−N−C) can satisfy the requirments

Received: May 7, 2022
Accepted: June 8, 2022
Published: June 23, 2022

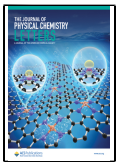

https://doi.org/10.1021/acs.jpclett.2c01381
J. Phys. Chem. Lett. 2022, 13, 5969−5976

mentioned above[29−32] and can serve as an ideal model system for studying the orbital dependence in catalytic reactions such as water splitting.

The water splitting through the hydrogen evolution reaction (HER) and OER is widely considered to be the most promising way toward a renewable hydrogen source for efficient energy conversion.[33−37] Meanwhile, they are the simplest catalytic reactions with clear reaction pathways. Therefore, the OER of Fe−N−C is employed in this work to study orbital dependence in catalytic reactions. The calculation results demonstrate that catalytic efficiency can be significantly regulated by adjusting the magnitude of the z-direction displacement (Δz) between the TM single atom and the N-doped graphene substrate. It is found that the d_{z^2} orbital participates primarily in the catalytic reaction, and the catalytic performance is determined mostly by the d_{z^2} orbital. The findings are expected to be generic according to our orbital-dependent formulization of the d-band theory. In addition, we have also investigated the HER and OER of TM−N−C (TM = Ti, V, Cr, Mn, Fe, or Co) systems via the density functional theory (DFT) approach and found that the Mn−N−C and Fe−N−C systems are the two best catalysts for HER and OER, which is consistent with some experiments. This work demonstrates that the catalytic reaction is indeed orbital-dependent, and the d-band theory could further be evolved by take orbital dependence into account. In this work, the energy position refers to the energy position relative to the Fermi level unless otherwise noted.

The TM−N−C system is gaining in popularity because of its high electrical conductivity and superior electrochemical stability in electrocatalytic applications.[28,29,38−41] In most cases, the TM single atom combines with the graphene double-vacancy sites containing four N substituents to form a porphyrin-like coordination environment and has a very good catalytic activity for various chemical reactions such as HER, oxygen reduction reaction (ORR), OER, etc.[30,31,42,43] As shown in Figure 1a, the TM single atom is located in the center

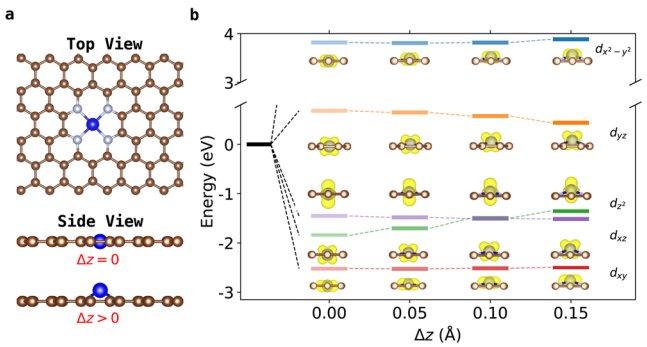

Figure 1. Atomic structure and d-band splitting diagram of TM−N−C. (a) Top and side views of the atomic structure of TM−N−C. (b) d-Band splitting of TM−N−C when there is a small displacement along the z-direction. The TM, nitrogen, and carbon atoms are colored blue, white, and gray, respectively.

of the crystal field formed by the four surrounding N atoms in the TM−N−C structure. Figure 1b shows that the degenerated d states of the TM single atom can be split into five d orbitals with different energies in the rectangular planar crystal field. The $d_{x^2-y^2}$ orbital has the highest energy because it is in a position opposite to the head of the N_4 ligand, which causes greater electrostatic repulsion of the electrons in the $d_{x^2-y^2}$ orbital than four other orbitals, while the other four orbitals are in the gap position of the N_4 ligand where the electrostatic repulsion of the electrons is weaker and the orbital energy level is lower. However, in most cases, the crystal field is not a rectangular plane because the TM single atom pops out to some extent as the atom is too large to fit into it. Moreover, when there is a small displacement along the z-direction ($\Delta z \neq 0$) between the TM single atom and N-doped graphene substrate in Figure 1a, the energy of the five orbitals will also change with the variation of Δz (Figure 1b). The energies of the d_{xz}, d_{yz}, and d_{z^2} orbitals change obviously with an increase in Δz, while those of d_{xy} and $d_{x^2-y^2}$ orbitals change slightly. The charge distributions of the d orbitals shift along the z-direction with the variation of Δz; then, the electrostatic repulsion of the d electrons changes, and finally, the energies of the d orbitals vary.

As the d orbitals can be adjusted via the crystal field, and the d states are single-atom-like (discrete lines, not bands) in TM−N−C. Hence, we expect it will provide us a feasible model structure for clearly investigating the orbital dependence of electrocatalytic reactions. In most of the ionic compounds, there is a hybridization between the orbitals between the TM and anion. The hybridization blends the electron of the d shell from the cation with the p shell from the anion together; hence, it is not easy to distinguish the d suborbitals. The TM−N−C system serves as an excellent model system to demonstrate the orbital dependence as the orbitals are single-atom-like. Therefore, in this report, we explore the orbital dependence in single-atom electrocatalytic reactions by studying the OER of water decomposition catalyzed by the Fe−N−C system.

Fe−N−C as the best catalyst for OER is chosen to unveil the underlying relationship between Δz and catalytic activity, and the OER catalytic efficiency versus Δz is investigated for Δz values in the range of 0−0.15 Å. Figure 2a shows the free energy diagram of the OER, and one can see that in the four steps (*OH, *O, *OOH, and *O_2) of OER, the free energy (ΔG) of *OOH increases with Δz; in the other three steps (*OH, *O, and *O_2), ΔG decreases with Δz. More

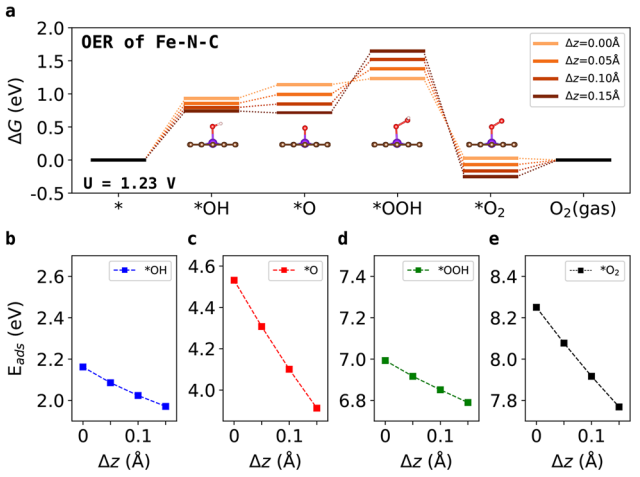

Figure 2. Catalytic efficiency of Fe−N−C regulated via vertical displacement. (a) Free energy diagram of Fe−N−C with Δz in the range of 0−0.15 Å. The illustration shows the stable structure of each step in the OER process. (b−e) E_{ads} values of four intermediate states (*OH, *O, *OOH, and *O_2) that vary with the Δz of Fe−N−C.

https://doi.org/10.1021/acs.jpclett.2c01381
J. Phys. Chem. Lett. 2022, 13, 5969−5976

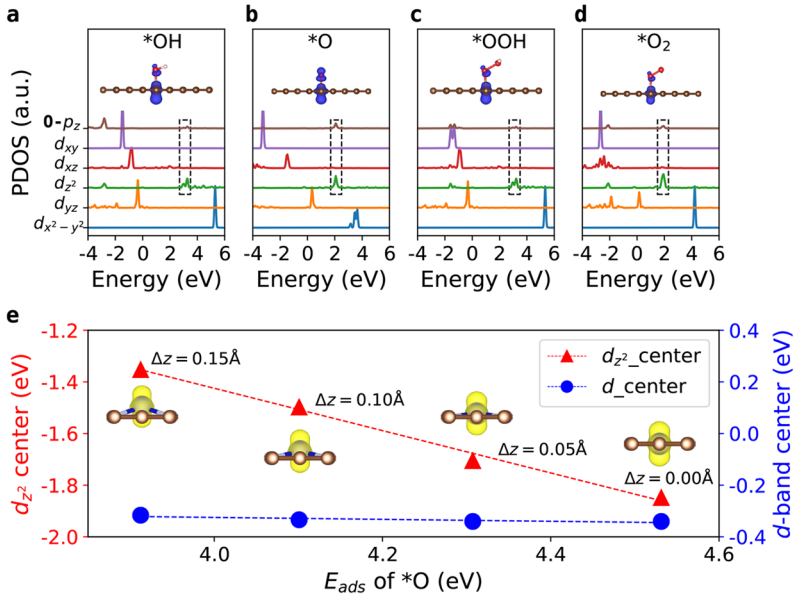

Figure 3. Only the d_{z^2} orbital participates in the OER. (a–d) Partial density of states (PDOS) and orbital hybridizations of the four intermediate states (*OH, *O, *OOH, and $*O_2$, respectively) in the OER process of Fe–N–C. (e) O atom adsorption energies correlate with the Fe d_{z^2} orbital center and the d-band center as Δz of Fe–N–C gradually increases from 0 to 0.15 Å. The illustration shows the shape of the Fe d_{z^2} orbital varies with Δz.

importantly, the ΔG values of *O and *OOH decrease when Δz increases from 0 to 0.15 Å. The overpotential increases from 1.23 to 1.64 V when Δz varies from 0 to 0.15 Å. The rate-determining step (RDS) is *OOH, but it will be replaced by *O if Δz continues to increase. In other words, the catalytic efficiency of the OER is fairly sensitive to the Δz of the TM single atom, and we can regulate the catalytic efficiency by adjusting Δz. As shown in Figure 2b–e, the adsorption energies (E_{ads}) of the four intermediate steps in OER all decrease linearly with Δz, which satisfies the "scaling relations" to some extent, but E_{ads} changes as a function of Δz at different rates, E_{ads} of *OH decreases from 2.16 to 1.97 eV, and E_{ads} of *OOH decreases from 6.99 to 6.79 eV. However, E_{ads} decreases from 4.53 to 3.91 eV and from 8.25 to 7.77 eV for *O and $*O_2$, respectively, much more quickly than that of *OH and *OOH. Hence, the ΔG values drift in the opposite direction for the *O and *OOH steps.

The d-band model states that the adsorption energy of an atom or a molecule on surface is a function of the d-band position.[3] The higher the d-band center in energy, the greater the adsorption energy. In most cases, the d-band of the catalyst is a wide band, composed by several broad d orbitals, and the broadening of the d orbitals is caused by the crystal field as well as the orbital hybridization between atoms. Hence, it is difficult to quantitatively analyze the magnitude of the participation of each sub-d orbital in the traditional catalytic reactions. However, in a single-atom catalyst, such as TM–N–C, the d-band of the TM single atom splits into discrete energy levels (d orbitals), and each sub-d orbital has a distinct energy level; therefore, the single-atom catalyst serves as an ideal model system to showcase which sub-d orbital participates in how much in the catalytic reactions. Because the TM atom may pop out of the planar configuration of TM–N–C, such structural symmetry breaking could degenerate d orbitals and shift their energy levels and, in turn, change the catalytic performance of the system. Therefore, we can further study the orbital dependence of catalytic reactions under structural perturbation. As presented below, Fe–N–C is adopted as it has good catalytic activity that has been confirmed experimentally[44−46] and theoretically (reported in this work), and the underlying mechanism is generally applicable for other absorption intermediates throughout the entire OER/HER process of any system.

The interactions between the molecule and surface occur primarily through the formation of bonding and antibonding states between the molecular orbitals and surfaces. For the OER of Fe–N–C, the four intermediate states interact with the surface via the hybridization of the O p_z and Fe d_{z^2} orbitals upon formation of very strong antibonding states at the energy position near 2.5 eV, as shown in Figure 3a–d. The other four Fe orbitals ($d_{x^2-y^2}$, d_{xz}, d_{yz}, and d_{xy}) have no obvious interaction with the adsorbed molecules, which means that only the d_{z^2} orbital participates in the reaction during the OER process. In addition, it is found that the energy position of the d_{z^2} orbital changed more significantly than the other four orbitals when Δz was gradually changed. The adsorption energy of *O has a linear correlation with the energy position of the d_{z^2} orbital center, as shown in Figure 3e, which is an extension of d-band theory. The higher the energy of the d_{z^2} orbital center, the lower the adsorption energy of the O atom. Figure 3e shows the charge distribution of the d_{z^2} orbital is pulled out of the surface as the Δz of the Fe single atom increases from 0 to 0.15 Å. As a result, the overlap between the Fe d_{z^2} and O p_z orbitals increases, and thus, the interaction between the adsorbed O atom and the Fe–N–C surface is enhanced.

When an O atom is adsorbed on the surface, the 2p states of O hybridize with the 3d states of TM by forming bonding and antibonding states, as shown in Figure 3b. To give a quantitative description of the relationship between the oxygen adsorption energy and electronic structure of TM–N–C, on the basis of the effective medium theory, a quantitative description, ΔE_{ts}, the energy difference due to the O 2p state coupled with the TM d-band state in the freezing potential approximation, is obtained by introducing an approximate

https://doi.org/10.1021/acs.jpclett.2c01381
J. Phys. Chem. Lett. 2022, 13, 5969–5976

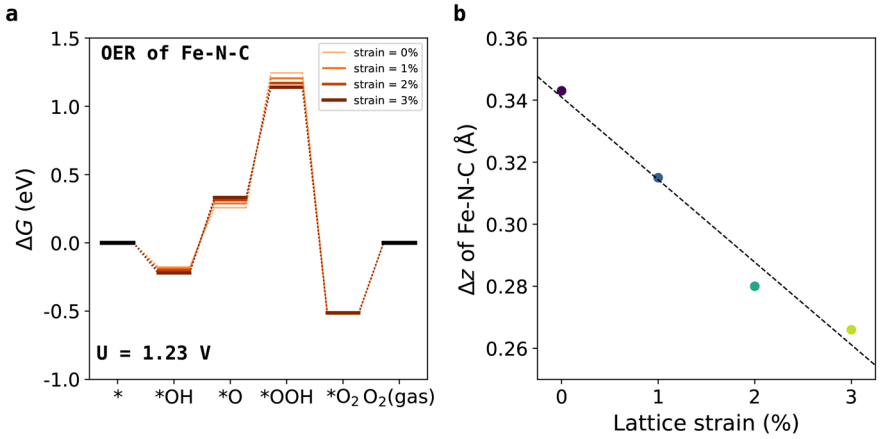

Figure 4. Lattice strain regulates the OER catalytic reactivity of Fe−N−C. (a) OER catalytic efficiency of the Fe−N−C system with change in strain from 0% to 3%. (b) Relationship between lattice strain and Δz of the *O step.

reactivity measure.[1,8] For the adsorption of an O atom on the TM−N−C surface, ΔE_{ts} is calculated as follows:

$$\Delta E_{ts} = \sum_i -2(1-f)\frac{V^2}{\varepsilon_{d_i} - \varepsilon_O} + \sum_i \alpha V^2 \quad (1)$$

where ε_O and ε_{d_i} represent the energy positions of the O 2p and TM 3d states, respectively, and f is the filling degree of the antibonding state. The first term of eq 1 describes the energy gain due to the hybridization between the O 2p and TM 3d states, and our calculations show that only the d_{z^2} states of TM can hybridize with the O 2p states, so d_i contain only d_{z^2}. The second term is the repulsion due to the orthogonalization of the O 2p and TM 3d states. V is the coupling matrix element, which can be written in the following form:

$$V = \eta\frac{M_O M_d}{r^3} \quad (2)$$

where M_O and M_d are given by the potential around the oxygen and TM, respectively, which depend on only the element type,[7] η is a constant independent of the TM, and r is the distance between the O and TM atom. Upon substitution of eq 2 into eq 1, it is found that the energy position of the d_{z^2} orbital is the most important parameters for determining the OER reactivity. Therefore, the center of the d_{z^2} orbital is chosen as the descriptor of the OER reactivity.

In general, a fairly complete picture can be illustrated here for TM single-atom catalysts: the catalytic activity of TM single-atom catalysts for the OER is correlated with the strength of the oxygen−TM bond. The energy position of the unperturbed TM d_{z^2} orbital center can be used as a good indicator of OER reactivity. The conventional d-band model still works but may not be accurate enough in this regime as the reaction has orbital dependence.

The results presented above prove that the catalytic reactivity can be significantly modified by changing the Δz between the TM single-atom catalysts and the N-doped graphene substrate. It is our hope that the theoretical scheme can provide a possible route via the structural perturbation for tuning of experimental catalytic activity. For example, the structural perturbation (Δz) can be achieved by applying a certain surface stress or external magnetic field. To demonstrate such a phenomenon, the OER catalytic efficiency of the Fe−N−C system under strain is calculated, as shown in Figure 4. The OER catalytic efficiency of Fe−N−C changes significantly after tensile stress is added to the N-doped graphene surface. The overpotential decreases from 1.24 to 1.14 eV with an increase in strain from 0% to 3%, as shown in Figure 4a. This is true because once stress is added to the substrate, the TM single atom is pulled out of the substrate surface during the reactions. Figure 4b shows the relationship between the lattice strain and Δz for the *O intermediate state in the OER of Fe−N−C. One can see that the lattice strain is linearly related to Δz, and the Δz of *O decreases from 0.34 to 0.26 Å with an increase in strain from 0% to 3%. Then the regulation of the catalytic activity is achieved by means of strain.

It is worth mentioning that, in the same way, the external magnetic field can also be used to regulate the catalytic activity. In a recent paper, Jin et al. discovered that the ORR activity of isolated Fe−N_4 single-atom catalysts changes as a function of the intersite distance.[47] It is likely that the intersite distance modulates the strain in the system and in turn adjusts the catalytic performance according to our theory. We will be performing further calculations to confirm it in a separate work.

In the TM surface system, the d state is a band with a certain width and participates as a whole in the catalytic reaction. Thus, the energy position of the d-band center is a good descriptor to reflect the electrocatalytic reactivity. However, in the TM−N−C system, the d-band split into five partial d orbitals due to the rectangular planar crystal field, and only the d_{z^2} orbital participates in the catalytic reaction. Therefore, the energy position of the d_{z^2} orbital center is a better descriptor of the electrocatalytic reactivity than that of the d-band center, which can be observed in Figure 3e. The energy position of the d-band center does not change when Δz of Fe−N−C increases from 0 to 0.15 Å, while that of the d_{z^2} orbital center obviously varies with Δz.

Previous studies have reported that the catalytic activity of a TM single atom is mainly related to the participation of d electrons.[42] It is clear that the catalytic activities of TM SACs are dependent on the TM species as they have distinct radii and numbers of d electrons. We first explore the catalytic activities (HER and OER) of TM−N−C with six different 3d TM species, which are Ti, V, Cr, Mn, Fe, and Co. As described previously,[31] we assume a two-step HER mechanism through *H and $*H_2$ and a four-step OER mechanism through *OH,

https://doi.org/10.1021/acs.jpclett.2c01381
J. Phys. Chem. Lett. 2022, 13, 5969−5976

*O, *OOH, and *O_2, as shown in Figure S1, and the ΔG values of the reaction intermediates are calculated to evaluate the catalytic activity. Two cases were considered here: allowing and disallowing the structural relaxation of TM−N−C during catalytic reaction. When the adsorbate is weakly bonded with the surface of TM−N−C and does not cause much structural deformation, all of the atoms, except the small molecule, of TM−N−C are fixed during the structural optimization. As shown in panels a and b of Figure S2, one can observe that the catalytic activity is TM-dependent for both the HER and the OER. For the HER, Mn−N−C has the highest catalytic activity with an overpotential of 0.13 V while Cr−N−C has the lowest catalytic activity with an overpotential of 0.83 V. For the OER, Fe−N−C is the best catalyst with an overpotential of 1.23 V while V−N−C is the worst with an overpotential of 3.55 V. When the adsorbate is strongly bonded with TM−N−C, as observed in the real world, the structure of TM−N−C is deformable as the reaction occurs; therefore, the position of atoms should be relaxed freely to capture structural deformation. Panels c and d of Figure S2 show the free energy diagram of HER and OER on fully relaxed TM−N−C, and the overall trend is fairly close to the fixed structure case. Mn−N−C and Cr−N−C with overpotentials of 0.04 and 0.73 V are still the best and worst catalysts, respectively, for the HER, while Fe−N−C and V−N−C with overpotentials of 1.78 and 3.07 V remain the best and worst catalysts, respectively, for the OER. Upon combination of the results of the two cases, Mn−N−C and Fe−N−C are likely the best catalysts for HER and OER, respectively, which is in good agreement with some experimental observations.[48−50]

Upon comparison of these two cases, the catalytic efficiency of each TM−N−C changes notably. For the HER and OER, the overpotentials of Ti−N−C change from 0.15 to 0.50 V and from 3.11 to 1.92 V, respectively, which has the largest ΔG shift among the six TM−N−C systems, while the overpotentials of Co−N−C change from 0.23 to 0.33 V for the HER and from 2.11 to 2.15 V for the OER, which is the smallest ΔG shift among the six TM−N−C systems. DFT calculations demonstrate that, in TM−N−C systems, the local environment of the catalytic active site undergoes a structural deformation and a TM single atom moves back and forth along the z-direction during the reaction and in turn affects the catalytic activity significantly. The change in amplitude of the catalytic activity is positively correlated with the Δz of a TM single atom (see Figure S3). The magnitude of Δz for different TM−N−C systems is actually related to the atomic radius of the TM single atom. The larger the atomic radius, the larger Δz, vice versa (see Figure S3). Therefore, Δz can be utilized to tune the catalytic performance of TM−N−C.

In summary, we propose that TM−N−C can be used as an ideal model system to study the orbital dependence in the water splitting catalytic reaction and provide a strategy for adjusting the electrocatalytic activity by changing the z-direction displacement between the TM single atom and N-doped graphene substrate. The DFT results show that the OER catalytic reactivity can be significantly modified with the variation of the z-direction displacement, and such modification breaks the "scaling relations" in catalytic chemistry. We have also investigated the microscopic mechanism behind the regulation of the OER catalytic activity. It is found that only the d_{z^2} orbital of the TM single atom participates in the reaction, and the energy position of the d_{z^2} orbital center can be used as a good indicator of OER reactivity. In addition, our calculations also indicate that lattice strain can be used as a good way to tune the z-direction displacement and thus regulate the catalytic activity. The results are expected to be generally applicable to other TM SACs, which provide an efficient way to tune the catalytic efficiency and achieve their applications in industrial catalysis.

COMPUTATIONAL METHODS

The plane-wave pseudopotential DFT calculations are performed by using the "Vienna ab initio Simulation Package" (VASP) code.[51−53] The geometry optimizations are performed with the Perdew−Burke−Ernzerhof (PBE) functional with generalized gradient approximation (GGA),[54] and the total energy and electronic structure calculations are performed with the Heyd−Scuseria−Ernzerhof (HSE) hybrid functional.[55,56] The electron−ion interaction is described by using the projector-augmented wave method.[57] The atomic structures are relaxed by using a conjugate gradient scheme until the maximum force on each atom is <0.02 eV $Å^{-1}$, and the energy cutoff is 500 eV. TM−N−C is simulated using a 6 × 6 graphene sheet (14.806 Å × 14.806 Å) with a TM single atom bonding to four N atoms in the double vacancy of graphene. A vacuum space of ∼20 Å along the z-direction is used to separate the interaction between the neighboring slabs. The 1 × 1 × 1 k-mesh is chosen to sample the Brillouin zone during PBE geometry optimization, while the 3 × 3 × 1 k-mesh for the HSE electronic structure calculation.

The HER has a two-step mechanism through *H and *H_2, and the OER has a four-step mechanism through *OH, *O, *OOH, and *O_2. For each step of the HER and OER, ΔG is defined as the difference in free energy between the initial and final states, and the rate-determining step (RDS) and overpotentials can be obtained by examining the reaction free energy of the different elementary steps. The HER includes the following steps:

$$* + H^+ + e^- \rightarrow *H \tag{3}$$

$$*H + H^+ + e^- \rightarrow H_2(g) + * \tag{4}$$

The OER occurs via the following steps:

$$H_2O + * \rightarrow *OH + H^+ + e^- \tag{5}$$

$$*OH \rightarrow *O + H^+ + e^- \tag{6}$$

$$*O + H_2O \rightarrow *OOH + H^+ + e^- \tag{7}$$

$$*OOH \rightarrow * + O_2(g) + H^+ + e^- \tag{8}$$

where * represents the adsorption site of the intermediate on the TM−N−C surface. The adsorption energies (E_{ads}) of *OH, *O, *OOH, and *O_2 are calculated by using the following equations:

$$E_{ads}(*OH) = G(*OH) - G(*) - [G(H_2O) - 1/2G(H_2)] \tag{9}$$

$$E_{ads}(*O) = G(*O) - G(*) - [G(H_2O) - G(H_2)] \tag{10}$$

$$E_{ads}(*OOH) = G(*OOH) - G(*) - [2G(H_2O) - 3/2G(H_2)] \tag{11}$$

$$E_{ads}(*O_2) = G(*O_2) - G(*) - [2G(H_2O) - 2G(H_2)] \tag{12}$$

https://doi.org/10.1021/acs.jpclett.2c01381
J. Phys. Chem. Lett. 2022, 13, 5969−5976

where $G(*)$, $G(*OH)$, $G(*O)$, $G(*OOH)$, and $G(*O_2)$ are the ground state energies of a clean TM−N−C surface and surfaces adsorbed with the four intermediate states, respectively, and $G(H_2O)$ and $G(H_2)$ are the DFT-calculated energies of H_2O and H_2, respectively.

The free energy difference (ΔG) of each step is calculated by the following equation:

$$\Delta G = \Delta E + \Delta \mathrm{ZPE} - T\Delta S + \Delta G_U + \Delta G_{pH} \quad (13)$$

where ΔE is the total energy difference between the reactants and products of the reactions, ΔZPE is the zero-point energy correction, ΔS is the vibrational entropy change at finite temperature T, $\Delta G_U = -eU$, where e is the elementary charge and U is the potential difference from the standard electrode potential, and ΔG_{pH} represents the effect of pH on the free energy. In this report, the U value of HER is 0 V and the U value of OER is 1.23 V.

Overpotential η of HER and OER can be evaluated from the ΔG of each step as

$$\eta_1 = \frac{\Delta G_H}{e} \quad (14)$$

$$\eta_2 = \frac{\max\{\Delta G_1, \Delta G_2, \Delta G_3, \Delta G_4\}}{e} \quad (15)$$

where ΔG_H is the free energy difference for HER and ΔG_1, ΔG_2, ΔG_3, and ΔG_4 are the free energy differences for the OER. More details of the calculations can be found in the Supporting Information.

■ ASSOCIATED CONTENT

Supporting Information

The Supporting Information is available free of charge at https://pubs.acs.org/doi/10.1021/acs.jpclett.2c01381.

Additional calculation details of the free energy and adsorption energy for HER and OER, supplementary figures of reaction path diagrams for HER and OER in the TM−N−C system, free energy diagrams of HER and OER in flat and buckled TM−N−C (TM = Ti, V, Cr, Mn, Fe, or Co), and diagrams of the overpotential, atomic radius, and Δz in six different kinds of TM−N−C systems (PDF)

■ AUTHOR INFORMATION

Corresponding Authors

Sheng Meng − *Songshan Lake Materials Laboratory, Dongguan, Guangdong 523808, China; Beijing National Laboratory for Condensed Matter Physics and Institute of Physics, Chinese Academy of Sciences, Beijing 100190, China;* orcid.org/0000-0002-1553-1432; Email: smeng@iphy.ac.cn

Miao Liu − *Songshan Lake Materials Laboratory, Dongguan, Guangdong 523808, China; Beijing National Laboratory for Condensed Matter Physics and Institute of Physics, Chinese Academy of Sciences, Beijing 100190, China; Center of Materials Science and Optoelectronics Engineering, University of Chinese Academy of Sciences, Beijing 100049, China;* orcid.org/0000-0002-1843-9519; Email: mliu@iphy.ac.cn

Authors

Yanan Wang − *Songshan Lake Materials Laboratory, Dongguan, Guangdong 523808, China; Beijing National Laboratory for Condensed Matter Physics and Institute of Physics, Chinese Academy of Sciences, Beijing 100190, China;* orcid.org/0000-0002-8436-0374

Yingzong Liang − *Songshan Lake Materials Laboratory, Dongguan, Guangdong 523808, China; Beijing National Laboratory for Condensed Matter Physics and Institute of Physics, Chinese Academy of Sciences, Beijing 100190, China*

Tao Bo − *Songshan Lake Materials Laboratory, Dongguan, Guangdong 523808, China; Beijing National Laboratory for Condensed Matter Physics and Institute of Physics, Chinese Academy of Sciences, Beijing 100190, China*

Complete contact information is available at: https://pubs.acs.org/10.1021/acs.jpclett.2c01381

Notes

The authors declare no competing financial interest.

■ ACKNOWLEDGMENTS

This work was supported by the National Key R&D Program of China (2021YFA0718700) and the Chinese Academy of Sciences (CAS-WX2021PY-0102, ZDBS-LY-SLH007, and XDB33020000). This research was also supported by the funding from the China Postdoctoral Science Foundation (2019TQ0347) and the Guangdong Basic and Applied Basic Research Foundation (2020A1515110743). The computational resources were provided by the Platform for Data-Driven Computational Materials Discovery of the Songshan Lake Materials Laboratory.

■ REFERENCES

(1) Hammer, B.; Nørskov, J. K. Electronic Factors Determining the Reactivity of Metal Surfaces. *Surf. Sci.* **1995**, *343*, 211−220.

(2) Hammer, B.; Nørskov, J. K. Theoretical Surface Science and Catalysis - Calculations and Concepts. *Adv. Catal.* **2000**, *45*, 71−129.

(3) Hammer, B.; Nørskov, J. K. Why Gold Is the Noblest of All the Metals. *Nature* **1995**, *376*, 238−240.

(4) Nørskov, J. K.; Abild-Pedersen, F.; Studt, F.; Bligaard, T. Density Functional Theory in Surface Chemistry and Catalysis. *Proc. Natl. Acad. Sci. U.S.A.* **2011**, *108*, 937−943.

(5) Pettersson, L. G. M.; Nilsson, A. A Molecular Perspective on the *d*-Band Model: Synergy Between Experiment and Theory. *Top. Catal.* **2014**, *57*, 2−13.

(6) Nilsson, A.; Pettersson, L. G. M.; Hammer, B.; Bligaard, T.; Christensen, C. H.; Nørskov, J. K. The Electronic Structure Effect in Heterogeneous Catalysis. *Catal. Lett.* **2005**, *100*, 111−114.

(7) Jacobsen, K. W.; Nørskov, J. K.; Puska, M. J. Interatomic Interactions in the Effective-Medium Theory. *Phys. Rev. B* **1987**, *35*, 7423−7442.

(8) Nørskov, J. K. Effective Medium Potentials for Molecule-Surface Interactions: H_2 on Cu and Ni Surfaces. *J. Chem. Phys.* **1989**, *90*, 7461−7471.

(9) Jacobsen, K. W.; Stoltze, P.; Nørskov, J. K. A Semi-Empirical Effective Medium Theory for Metals and Alloys. *Surf. Sci.* **1996**, *366*, 394−402.

(10) Anderson, P. W. Localized Magnetic States in Metals. *Phys. Rev.* **1961**, *124*, 41−53.

(11) Newns, D. M. Self-Consistent Model of Hydrogen Chemisorption. *Phys. Rev.* **1969**, *178*, 1123−1135.

(12) Mavrikakis, M.; Hammer, B.; Nørskov, J. K. Effect of Strain on the Reactivity of Metal Surfaces. *Phys. Rev. Lett.* **1998**, *81*, 2819−2822.

(13) Kibler, L. A.; El-Aziz, A. M.; Hoyer, R.; Kolb, D. M. Tuning Reaction Rates by Lateral Strain in a Palladium Monolayer. *Angew. Chem., Int. Ed.* **2005**, *44*, 2080−2084.
(14) Vojvodic, A.; Nørskov, J. K.; Abild-Pedersen, F. Electronic Structure Effects in Transition Metal Surface Chemistry. *Top. Catal.* **2014**, *57*, 25−32.
(15) Bhattacharjee, S.; Waghmare, U. V.; Lee, S. C. An Improved *d*-Band Model of the Catalytic Activity of Magnetic Transition Metal Surfaces. *Sci. Rep.* **2016**, *6*, 35916.
(16) Suntivich, J.; May, K. J.; Gasteiger, H. A.; Goodenough, J. B.; Yang, S. H. A Perovskite Oxide Optimized for Oxygen Evolution Catalysis from Molecular Orbital Principles. *Science* **2011**, *334*, 1383−1385.
(17) Zhang, J.; Qu, L.; Shi, G.; Liu, J.; Chen, J.; Dai, L. N,P-Codoped Carbon Networks as Efficient Metal-Free Bifunctional Catalysts for Oxygen Reduction and Hydrogen Evolution Reactions. *Angew. Chem., Int. Ed.* **2016**, *55*, 2230−2234.
(18) Zhang, J.; Zhao, Z.; Xia, Z.; Dai, L. A Metal-Free Bifunctional Electrocatalyst for Oxygen Reduction and Oxygen Evolution Reactions. *Nat. Nanotechnol.* **2015**, *10*, 444−452.
(19) Petrie, J. R.; Cooper, V. R.; Freeland, J. W.; Meyer, T. L.; Zhang, Z.; Lutterman, D. A.; Lee, H. N. Enhanced Bifunctional Oxygen Catalysis in Strained $LaNiO_3$ Perovskites. *J. Am. Chem. Soc.* **2016**, *138*, 2488−2491.
(20) Liang, Y.; Li, Y.; Wang, H.; Zhou, J.; Wang, J.; Regier, T.; Dai, H. Co_3O_4 Nanocrystals on Graphene as a Synergistic Catalyst for Oxygen Reduction Reaction. *Nat. Mater.* **2011**, *10*, 780−786.
(21) Liu, Q.; Jin, J.; Zhang, J. $NiCo_2S_4$@Graphene as a Bifunctional Electrocatalyst for Oxygen Reduction and Evolution Reactions. *ACS Appl. Mater. Interfaces* **2013**, *5*, 5002−5008.
(22) Zhao, Y.; Chen, S.; Sun, B.; Su, D.; Huang, X.; Liu, H.; Yan, Y.; Sun, K.; Wang, G. Graphene-Co_3O_4 Nanocomposite as Electrocatalyst with High Performance for Oxygen Evolution Reaction. *Sci. Rep.* **2015**, *5*, 7629.
(23) Shi, Y.; Prezhdo, O. V.; Zhao, J.; Saidi, W. A. Iodine and Sulfur Vacancies Cooperation Promotes Ultrafast Charge Extraction at $MAPbI_3/MoS_2$ Interface. *ACS Energy Lett.* **2020**, *5*, 1346−1354.
(24) Zhao, X.; Liu, Y. Unveiling the Active Structure of Single Nickel Atom Catalysis: Critical Roles of Charge Capacity and Hydrogen Bonding. *J. Am. Chem. Soc.* **2020**, *142*, 5773−5777.
(25) Kaiser, S. K.; Chen, Z.; Faust Akl, D.; Mitchell, S.; Pérez-Ramírez, J. Single-Atom Catalysts across the Periodic Table. *Chem. Rev.* **2020**, *120*, 11703−11809.
(26) Hossain, M. D.; Liu, Z.; Zhuang, M.; Yan, X.; Xu, G. L.; Gadre, C. A.; Tyagi, A.; Abidi, I. H.; Sun, C. J.; Wong, H.; et al. Rational Design of Graphene-Supported Single Atom Catalysts for Hydrogen Evolution Reaction. *Adv. Energy Mater.* **2019**, *9*, 1803689.
(27) Bo, T.; Liu, Y.; Yuan, J.; Wu, P.; Zhou, W. Tunable HER Activity from Doping and Strain Strategies for *β*-Sb Monolayer: DFT Calculations. *Comput. Mater. Sci.* **2020**, *185*, 109966.
(28) Bezerra, C. W. B.; Zhang, L.; Lee, K.; Liu, H.; Marques, A. L. B.; Marques, E. P.; Wang, H.; Zhang, J. A Review of Fe-N/C and Co-N/C Catalysts for the Oxygen Reduction Reaction. *Electrochim. Acta* **2008**, *53*, 4937−4951.
(29) Fei, H.; Dong, J.; Arellano-Jiménez, M. J.; Ye, G.; Dong Kim, N.; Samuel, E. L. G.; Peng, Z.; Zhu, Z.; Qin, F.; Bao, J.; et al. Atomic Cobalt on Nitrogen-Doped Graphene for Hydrogen Generation. *Nat. Commun.* **2015**, *6*, 8668.
(30) Zitolo, A.; Goellner, V.; Armel, V.; Sougrati, M.-T.; Mineva, T.; Stievano, L.; Fonda, E.; Jaouen, F. Identification of Catalytic Sites for Oxygen Reduction in Iron- and Nitrogen-Doped Graphene Materials. *Nat. Mater.* **2015**, *14*, 937−942.
(31) Zhang, L.; Jia, Y.; Gao, G.; Yan, X.; Chen, N.; Chen, J.; Soo, M.; Wood, B.; Yang, D.; Du, A.; et al. Graphene Defects Trap Atomic Ni Species for Hydrogen and Oxygen Evolution Reactions. *Chem.* **2018**, *4*, 285−297.
(32) Fei, H.; Dong, J.; Feng, Y.; Allen, C. S.; Wan, C.; Volosskiy, B.; Li, M.; Zhao, Z.; Wang, Y.; Sun, H.; et al. General Synthesis and Definitive Structural Identification of MN_4C_4 Single-Atom Catalysts with Tunable Electrocatalytic Activities. *Nat. Catal.* **2018**, *1*, 63−72.
(33) Cady, C. W.; Gardner, G.; Maron, Z. O.; Retuerto, M.; Go, Y. B.; Segan, S.; Greenblatt, M.; Dismukes, G. C. Tuning the Electrocatalytic Water Oxidation Properties of AB_2O_4 Spinel Nanocrystals: A (Li, Mg, Zn) and B (Mn, Co) Site Variants of $LiMn_2O_4$. *ACS Catal.* **2015**, *5*, 3403−3410.
(34) Xu, Y.; Rao, H.; Wang, X.; Chen, H.; Kuang, D.; Su, C. In-Situ Formation of Zinc Ferrite Modified Al-Doped ZnO Nanowire Arrays for Solar Water Splitting. *J. Mater. Chem. A* **2016**, *4*, 5124−5129.
(35) Zhang, B.; Zheng, X.; Voznyy, O.; Comin, R.; Bajdich, M.; Garcia-Melchor, M.; Han, L.; Xu, J.; Liu, M.; Zheng, L.; et al. Homogeneously Dispersed Multimetal Oxygen-Evolving Catalysts. *Science* **2016**, *352*, 333−337.
(36) Walter, M. G.; Warren, E. L.; McKone, J. R.; Boettcher, S. W.; Mi, Q. X.; Santori, E. A.; Lewis, N. S. Solar Water Splitting Cells. *Chem. Rev.* **2010**, *110*, 6446−6473.
(37) Luo, J.; Im, J. H.; Mayer, M. T.; Schreier, M.; Nazeeruddin, M. K.; Park, N. G.; Tilley, S. D.; Fan, H. J.; Gratzel, M. Water Photolysis at 12.3% Efficiency Via Perovskite Photovoltaics and Earth-Abundant Catalysts. *Science* **2014**, *345*, 1593−1596.
(38) Ma, R.; Lin, G.; Zhou, Y.; Liu, Q.; Zhang, T.; Shan, G.; Yang, M.; Wang, J. A Review of Oxygen Reduction Mechanisms for Metal-Free Carbon-Based Electrocatalysts. *npj Comput. Mater.* **2019**, *5*, 78.
(39) Kropp, T.; Mavrikakis, M. Transition Metal Atoms Embedded in Graphene: How Nitrogen Doping Increases Co Oxidation Activity. *ACS Catal.* **2019**, *9*, 6864−6868.
(40) Wang, H.; Wang, Q.; Cheng, Y.; Li, K.; Yao, Y.; Zhang, Q.; Dong, C.; Wang, P.; Schwingenschlögl, U.; Yang, W.; Zhang, X. X. Doping Monolayer Graphene with Single Atom Substitutions. *Nano Lett.* **2012**, *12*, 141−144.
(41) Yin, P.; Yao, T.; Wu, Y.; Zheng, L.; Lin, Y.; Liu, W.; Ju, H.; Zhu, J.; Hong, X.; Deng, Z.; et al. Single Cobalt Atoms with Precise N-Coordination as Superior Oxygen Reduction Reaction Catalysts. *Angew. Chem.* **2016**, *128*, 10958−10963.
(42) Yang, H.; Hung, S.; Liu, S.; Yuan, K.; Miao, S.; Zhang, L.; Huang, X.; Wang, H.; Cai, W.; Chen, R.; et al. Atomically Dispersed Ni(I) as the Active Site for Electrochemical CO_2 Reduction. *Nat. Energy* **2018**, *3*, 140−147.
(43) Yang, H.; Wu, Y.; Li, G.; Lin, Q.; Hu, Q.; Zhang, Q.; Liu, J.; He, C. Scalable Production of Efficient Single-Atom Copper Decorated Carbon Membranes for CO_2 Electroreduction to Methanol. *J. Am. Chem. Soc.* **2019**, *141*, 12717−12723.
(44) Deng, Q.; Zhao, J.; Wu, T.; Chen, G.; Hansen, H. A.; Vegge, T. 2D Transition Metal-TCNQ Sheets as Bifunctional Single-Atom Catalysts for Oxygen Reduction and Evolution Reaction (ORR/OER). *J. Catal.* **2019**, *370*, 378−384.
(45) Chen, J.; Li, H.; Fan, C.; Meng, Q.; Tang, Y.; Qiu, X.; Fu, G.; Ma, T. Dual Single-Atomic Ni-N_4 and Fe-N_4 Sites Constructing Janus Hollow Graphene for Selective Oxygen Electrocatalysis. *Adv. Mater.* **2020**, *32*, 2003134.
(46) Zhu, C.; Fu, S.; Song, J.; Shi, Q.; Su, D.; Engelhard, M. H.; Li, X.; Xiao, D.; Li, D.; Estevez, L.; et al. Self-Assembled Fe-N-Doped Carbon Nanotube Aerogels with Single-Atom Catalyst Feature as High-Efficiency Oxygen Reduction Electrocatalysts. *Small* **2017**, *13*, 1603407.
(47) Jin, Z.; Li, P.; Meng, Y.; Fang, Z.; Xiao, D.; Yu, G. Understanding the Inter-Site Distance Effect in Single-Atom Catalysts for Oxygen Electroreduction. *Nat. Catal.* **2021**, *4*, 615−622.
(48) Wang, M.; Fu, W.; Du, L.; Wei, Y.; Rao, P.; Wei, L.; Zhao, X.; Wang, Y.; Sun, S. Surface Engineering by Doping Manganese into Cobalt Phosphide Towards Highly Efficient Bifunctional HER and OER Electrocatalysis. *Appl. Surf. Sci.* **2020**, *515*, 146059.
(49) Sun, T.; Mitchell, S.; Li, J.; Lyu, P.; Wu, X.; Pérez-Ramírez, J.; Lu, J. Design of Local Atomic Environments in Single-Atom Electrocatalysts for Renewable Energy Conversions. *Adv. Mater.* **2021**, *33*, 2003075.
(50) Lei, C.; Chen, H.; Cao, J.; Yang, J.; Qiu, M.; Xia, Y.; Yuan, C.; Yang, B.; Li, Z.; Zhang, X.; et al. FeN_4 Sites Embedded into Carbon

https://doi.org/10.1021/acs.jpclett.2c01381
J. Phys. Chem. Lett. 2022, 13, 5969−5976

Nanofiber Integrated with Electrochemically Exfoliated Graphene for Oxygen Evolution in Acidic Medium. *Adv. Energy Mater.* **2018**, *8*, 1801912.
(51) Kresse, G.; Hafner, J. *Ab Initio* Molecular Dynamics for Liquid Metals. *Phys. Rev. B* **1993**, *47*, 558−561.
(52) Kresse, G.; Hafner, J. *Ab Initio* Molecular Dynamics for Open-Shell Transition Metals. *Phys. Rev. B* **1993**, *48*, 13115−13118.
(53) Kresse, G.; Hafner, J. *Ab Initio* Molecular-Dynamics Simulation of the Liquid-Metal-Amorphous-Semiconductor Transition in Germanium. *Phys. Rev. B* **1994**, *49*, 14251−14269.
(54) Perdew, J. P.; Burke, K.; Ernzerhof, M. Generalized Gradient Approximation Made Simple. *Phys. Rev. Lett.* **1996**, *77*, 3865−3868.
(55) Heyd, J.; Scuseria, G. E. Efficient Hybrid Density Functional Calculations in Solids: Assessment of the Heyd-Scuseria-Ernzerhof Screened Coulomb Hybrid Functional. *J. Chem. Phys.* **2004**, *121*, 1187−1192.
(56) Heyd, J.; Scuseria, G. E.; Ernzerhof, M. Hybrid Functionals Based on a Screened Coulomb Potential. *J. Chem. Phys.* **2003**, *118*, 8207−8215.
(57) Kresse, G.; Joubert, D. From Ultrasoft Pseudopotentials to the Projector Augmented-Wave Method. *Phys. Rev. B* **1999**, *59*, 1758−1775.

https://doi.org/10.1021/acs.jpclett.2c01381
J. Phys. Chem. Lett. 2022, 13, 5969−5976